Mon. Not. R. Astron. Soc. **315**, 635–645 (2000)

New views of Betelgeuse: multi-wavelength surface imaging and implications for models of hotspot generation

J. S. Young,[1]★ J. E. Baldwin,[1] R. C. Boysen,[1] C. A. Haniff,[1] P. R. Lawson,[1]†
C. D. Mackay,[2] D. Pearson,[1] J. Rogers,[1] D. St.-Jacques,[1]‡ P. J. Warner,[1] D. M. A. Wilson[1]
and R. W. Wilson[1]§

[1]*Astrophysics Group, Cavendish Laboratory, Madingley Road, Cambridge CB3 0HE*
[2]*Institute of Astronomy, Madingley Road, Cambridge CB3 0HA*

Accepted 2000 January 31. Received 1999 September 1

ABSTRACT

We report contemporaneous multi-wavelength interferometric imaging of the red supergiant star Betelgeuse (α Orionis), using the Cambridge Optical Aperture Synthesis Telescope (COAST) and the William Herschel Telescope (WHT), at wavelengths of 700, 905 and 1290 nm. We find a strong variation in the apparent symmetry of the stellar brightness distribution as a function of wavelength. At 700 nm the star is highly asymmetric, and can be modelled as the superposition of three bright spots on a strongly limb-darkened disc. However, at 905 nm only a single low-contrast feature is visible and at 1290 nm the star presents a featureless symmetric disc. The change in spot contrast with wavelength is consistent with a model in which the bright spots represent unobscured areas of elevated temperature, owing perhaps to convection, on a stellar disc that itself has a different appearance, i.e. geometrical extent and limb-darkening profile, at different wavelengths. The featureless centre-to-limb brightness profile seen at 1290 nm is consistent with this model and suggests that future interferometric monitoring of the star to quantify the size changes associated with radial velocity variations should be performed at similar wavelengths in the near-infrared.

Key words: techniques: interferometric – telescopes – stars: imaging – stars: individual: Betelgeuse – stars: late-type – stars: variables: other.

1 INTRODUCTION

The large apparent size and prodigious luminosity of the red supergiant Betelgeuse (α Orionis) have in the past made it a favourite target for high angular resolution imaging experiments. These have provided conclusive evidence that its optical brightness distribution is far from uniform, and in particular have suggested that it can be modelled as the superposition of a small number (1–3) of bright unresolved features on an otherwise symmetric disc (see, e.g. Buscher et al. 1990; Wilson et al. 1992; Klückers et al. 1997; Tuthill, Haniff & Baldwin 1997). Typically the compact features contribute 10–20 per cent of the total flux from the system and both their brightnesses and locations on the stellar disc appear to change on time-scales of months (Wilson, Dhillon & Haniff 1997). However, despite the frequency of their detection, there is still no consensus as to their origin (see, e.g. the discussion in Uitenbroek, Dupree & Gilliland 1998).

One of the favoured explanations for these 'hotspots' is that they are manifestations of the giant convective granules predicted by Schwarzschild (1975), who suggested that the evolution of such structures, favoured under the conditions found in stars such as Betelgeuse, might produce the irregular photometric variability seen in red giants and supergiants. The bright features seen in high resolution images would then correspond to the tops of convective plumes whose temperatures were enhanced with respect to the local stellar surface. The small number of hotspots seen, and their large contrast with respect to the stellar disc, are consistent with this picture, but a recent study by Wilson et al. (1997) found no relationship between the variations in hotspot flux and simultaneous changes in the total V band magnitude of Betelgeuse over a period of four months. Furthermore, such a model would have difficulties explaining the brightness asymmetries detected in the

★ E-mail: J.S.Young@mrao.cam.ac.uk
† Present address: Jet Propulsion Laboratory, 4800 Oak Grove Drive, Pasadena, CA 91109, USA.
‡ Present address: National Astronomical Observatory, 2-21-1 Osawa, Mitaka, Tokyo 181-8588, Japan.
§ On secondment from UK Astronomy Technology Centre, Royal Observatory, Edinburgh, Blackford Hill, Edinburgh EH9 3HJ, UK.

ultraviolet by the Hubble Space Telescope (Gilliland & Dupree 1996; Uitenbroek et al. 1998), where convection is likely to play a much smaller role in transporting energy as compared to the deeper photosphere.

In an effort to investigate possible models for the brightness asymmetries, we have carried out a campaign of contemporaneous interferometric measurements of Betelgeuse with the Cambridge Optical Aperture Synthesis Telescope (COAST) and the William Herschel Telescope (WHT) in La Palma. We report here measurements made in 1997 October and November using interferometer baselines of up to 3.7 m at the WHT and up to 8.9 m at COAST. These have allowed us to compare the stellar brightness distribution directly at three widely-spaced wavelengths (700, 905 and 1290 nm), and thereby investigate whether a convective origin for the hotspots is consistent with the measured change in contrast of the asymmetries as a function of wavelength.

2 OBSERVATIONS AND DATA REDUCTION

2.1 Measurements with COAST

2.1.1 *Observations*

Interferometric observations of Betelgeuse were secured during the months of 1997 October and November at COAST using bandpasses with effective wavelengths of 905 and 1290 nm and bandwidths (FWHM) of 50 and 150 nm respectively. The short-wave (optical) measurements used the standard COAST beam-combiner and avalanche photodiode (APD) detectors (Baldwin et al. 1994) while the 1290-nm observations were obtained with a separate pupil–plane combiner optimized for the *JHK* bands (Young et al. 1998; Young 1999). This feeds four pixels of a NICMOS3 detector which act as infrared analogues of the APDs.

For these observations, four of the five COAST telescopes were operational. At 905 nm these were stopped down to 16 cm to match the seeing conditions in Cambridge ($r_0 \sim 10$ cm at this wavelength), but for the 1290-nm measurements the full 40-cm telescope apertures were used. Observations of Betelgeuse were interleaved with observations of calibrator stars, either unresolved or of small and known diameters. To optimize the signal-to-noise ratio, the source visibilities were first measured separately on all the baselines on which fringes could be detected, each datum for analysis arising from 30–100 s of raw data. If at least three baselines were measurable and the atmospheric coherence time was sufficiently long, closure phase measurements were also secured, by recording fringes on three baselines simultaneously.

All the measurements were obtained using a single configuration of the COAST array, for which the maximum baseline was 9 m. This permitted good sampling of the visibility function of Betelgeuse at 1290 nm, but was not optimal for imaging at 905 nm. At this shorter wavelength, the star was heavily resolved on most of the interferometer baselines except at very early or late hour angles. As a result, most of the visibility amplitude and closure phase measurements obtained at this wavelength were made on a single triangle of baselines, none of which was longer than 7 m. Only four 905-nm visibility measurements were made using the full capability of the array, the longest projected baseline being 7.8 m. Further details of the observations are given in Table 1.

2.1.2 *Data reduction*

Reduction of the data, to obtain visibility amplitudes and closure phases, was performed using standard methods in which the power spectrum and bispectrum of the interference fringes were averaged over each dataset (Burns 1997; Burns et al. 1997). The raw data from both the optical and infrared correlators were treated similarly, and after averaging gave visibility amplitudes with formal fractional errors in the range 2–10 per cent of the values and closure phases with typical uncertainties of between 5° and 10°. These errors, however, include no contribution from calibration uncertainties, which primarily affect the visibility amplitudes. To accommodate potential changes in the seeing conditions between observations of the source and calibrator stars we have thus adjusted the error estimates on the visibilities. Depending upon the proximity on the sky and time of the source and calibrator observations, additional uncertainties of between 10 and 20 per cent of the visibility were assigned to the data.

2.2 Measurements with the WHT

2.2.1 *Observations*

Further interferometric observations of Betelgeuse were made on the nights of 1997 November 15 and 16 at the Ground-based High Resolution Imaging Laboratory (GHRIL) of the WHT. These used the non-redundant aperture masking method (Baldwin et al. 1986; Haniff et al. 1987) and employed an optical arrangement equivalent to that described by Buscher et al. (1990), in which a pupil–plane mask, opaque save for a non-redundant array of holes, is used to select a set of Fourier components for measurement. The resulting interference fringes were imaged on to a CCD and recorded at 12-ms intervals using on-chip binning to compress each two-dimensional snapshot into a single row of data. A linear

Table 1. Log of observations at COAST and the WHT. Dates refer to the start of the night of each set of observations. N_{vis} and N_{cl} are the number of visibility and closure-phase measurements made. An identical number of visibility measurements were made for the calibrator star(s). Each 'measurement' corresponds to 30–100 s of observations.

Date	Telescope	Baseline range (m)	700 nm		905 nm		1290 nm		Calibrator(s)
			N_{vis}	N_{cl}	N_{vis}	N_{cl}	N_{vis}	N_{cl}	
97/10/21	COAST	2.0–8.9	–	–	–	–	18	7	β Ori
97/10/24	COAST	2.3–7.5	–	–	10	4	–	–	γ Ori
97/10/31	COAST	2.3–6.9	–	–	5	1	–	–	β Ori
97/11/11	COAST	1.6–8.8	–	–	–	–	53	36	μ Gem
97/11/12	COAST	3.1–6.9	–	–	13	–	–	–	β Ori
97/11/15	WHT	0.3–3.7	90	90	–	–	–	–	γ Ori
97/11/16	WHT	0.3–3.7	–	–	60	60	–	–	γ Ori
97/11/21	COAST	1.6–7.7	–	–	29	9	–	–	β Ori, α CMi

five-hole mask was used, giving 10 baselines with lengths ranging between 0.3 and 3.7 m.

Measurements were made in two bandpasses, the first at 700 nm, with a bandwidth of 10 nm, and the second at 905 nm, i.e. the same 50-nm bandpass used at COAST. In order to sample the Fourier plane well, the aperture mask was rotated relative to the sky and 5000 short-exposure images were recorded at each of six or nine different position angles for both the source and the calibrator star, γ Ori. To assess the errors in the measurements, most of the observations at 700 nm were repeated. In all cases these gave very similar results. For consistency, however, the entries in Table 1 and the results presented here, all refer to a single dataset. Details of the observations are given in Table 1.

2.2.2 *Data reduction*

For each orientation of the mask, the fringe data were reduced using standard procedures (Haniff et al. 1987; Buscher et al. 1990) to give estimates of the visibility amplitudes on all 10 interferometer baselines and of the closure phases on the 10 (linear) triangles of baselines. As for the COAST measurements, the uncertainties on the visibility amplitudes were dominated by calibration errors, which in this instance were unusually large (fractional error ~30 per cent). On the other hand, the calibrated closure phase measurements were of very high quality, with typical errors of only 1°–3°, so that despite the poor quality of the visibility amplitude data the sensitivity of the experiment to detect small-scale structure remained high. The orientation and scale of the detector were determined by observations of two close visual binaries with well-determined orbits and had errors of a few per cent and 2° respectively.

3 RESULTS

3.1 General procedure

In view of the total amount of Fourier data collected at any given observing epoch (Table 1), we have used model fitting as the most efficient technique for extracting quantitative information about the structure of Betelgeuse's optical and near-infrared emission. Some of our data did, though, allow model-independent image reconstructions (see Section 3.2.3), and in these cases the images recovered provide an independent check on the reliability of the model-fitting procedure.

For each dataset, simple models for the source brightness distribution, consisting of a uniform or limb-darkened disc plus some number of Gaussian components (representing bright or dark spots of varying sizes), were fit to the visibility amplitudes and closure phases. A conjugate-gradient algorithm was employed to find the model parameters that minimized the χ^2 statistic, using a range of initial starting conditions to improve the chance of identifying a global minimum. Within this framework, the models were progressively increased in complexity until an acceptable fit, judged by the minimum χ^2 value, was found. Uncertainties (1σ) in the best-fitting model parameters were estimated from the curvatures of the χ^2 hyper-surfaces around minima, having accommodated any correlations between the different parameters.

In order to model the expected strong limb-darkening of Betelgeuse, the centre-to-limb brightness distribution was characterized using the empirical models of Hestroffer (1997). These are parametrized by a single limb-darkening coefficient α, but usefully describe a wide range of limb darkenings, from a uniform disc ($\alpha = 0$) to Gaussian-like profiles ($\alpha \approx 8$). More importantly, recent work (Hofmann & Scholz 1998) has shown that the profile with $\alpha = 1$ is a good fit to the intensity profiles calculated from the most up-to-date calculations of cool giant star photospheres.

The COAST and WHT observations reported here actually spanned an entire month. It is known that Betelgeuse's apparent brightness distribution can change, albeit not in a gross sense, on time-scales as short as three weeks (Wilson et al. 1997), so only a subset of the available 1290 and 905-nm data were used to investigate the comparative contrast of any surface features. The measurements from 1997 November 11 (1290 nm), 1997 November 21 (905 nm) and 1997 November 15 (700 nm) were thus used to investigate the colour dependence of the surface structure, while the full dataset was used to search for any temporal variation in the overall structure of the star.

3.2 Evidence for asymmetric structure

3.2.1 *Asymmetries at 1290 nm*

The visibilities and closure phases measured with COAST on 1997 November 11 at 1290 nm are shown in Fig. 1. At this wavelength

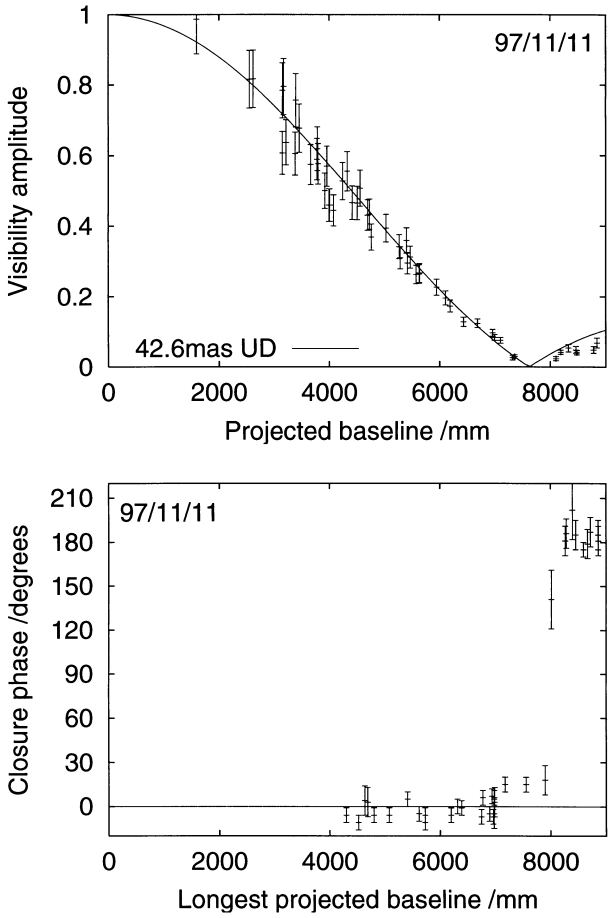

Figure 1. Calibrated visibilities and corresponding closure phases for Betelgeuse as observed at COAST at 1290 nm on 1997 November 11. The null in the visibility amplitude seen as the closure phase changes from ~0° to ~180° is indicative of a symmetric disc. The solid curve in the upper panel shows the predictions for a uniform disc model fit to the visibility amplitudes on baselines shorter than 7.5 m. The smaller measured visibilities seen beyond the first null of the model imply that the actual stellar disc is darkened towards the limb.

the calibrated visibility is approximately equal to unity at low spatial frequencies, and falls monotonically with increasing baseline length, until it reaches a minimum at a baseline of about 8 m, at which point the closure phase flips from ~0° to ~180°. Beyond this, the visibility amplitude rises once more out to the maximum baseline measured. This type of behaviour has a relatively simple explanation, i.e. that the brightness distribution can be modelled as an otherwise featureless symmetric disc.

This interpretation was confirmed by model fitting: a good fit to the Fourier data (reduced $\chi^2 = 1.8$) was obtained for a limb-darkened model with $\alpha = 1.3 \pm 0.1$ and a zero-intensity disc diameter of 51.4 ± 0.8 mas. Models with elliptical distributions of flux produced no improvement in χ^2, implying an axial ratio of two perpendicular diameters equal to 0.99 ± 0.01.

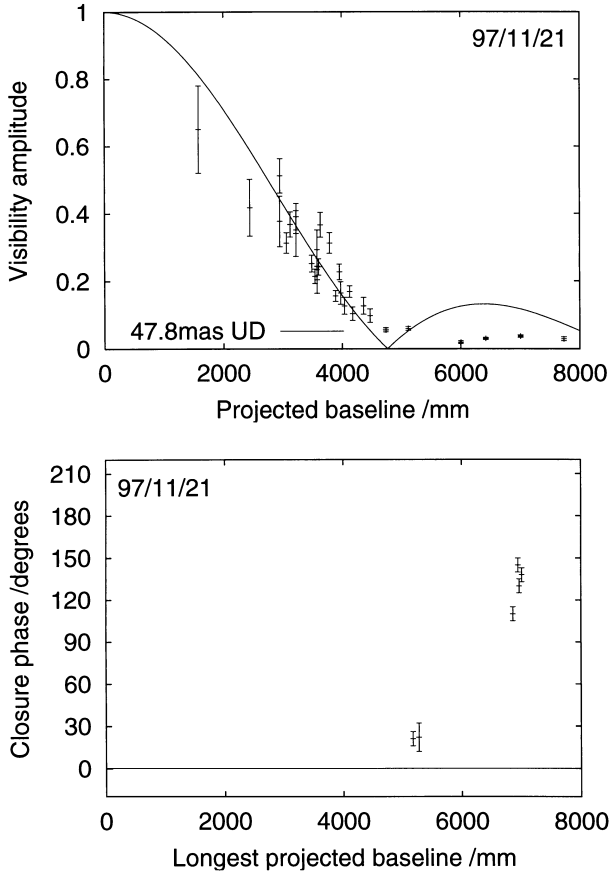

Figure 2. Visibility amplitudes and closure phases for Betelgeuse at 905 nm measured at COAST on 1997 November 21. Only those closure phases measured using the triangle of baselines linking the centre, east and north telescopes are shown. These are plotted against the projected length of the longest baseline in the triangle in the lower panel. In the top panel the solid curve shows the predictions of a uniform disc model that best fits the short baseline visibility amplitudes (diameter = 47.8 mas).

To investigate the possibility of any asymmetric component contributing to the apparent stellar brightness distribution, fits of a model consisting of a limb-darkened disc with $\alpha = 1$, whose diameter was a free parameter, plus one unresolved (10-mas FWHM) component were then carried out. Repeated trials always led to the compact feature being placed very close to the centre of the disc to conform to the measured closure phase variation, the 1σ upper limit to the flux of this feature being just 6 per cent of the total. However, despite the additional degrees of freedom introduced by this second component, none of these more complex models was able to fit the data any better than the $\alpha = 1.3$ disc mentioned above. Further modelling confirmed that, as expected, limits on the brightness of any compact features away from the disc centre were much smaller, and so the figure of six per cent represents a hard limit on the contrast of any unresolved structures present at 1290 nm.

3.2.2 *Asymmetries at 905 nm*

The possible presence of asymmetric structure in the brightness distribution of Betelgeuse at 905 nm was investigated using the COAST dataset from 1997 November 21. Most of the closure phase data secured on that night were obtained using a single triangle of baselines, and these measurements, together with the calibrated visibility amplitudes observed, are plotted in Fig. 2. Although displaying significantly more scatter than the 1290-nm data, the visibility function shows no evidence for a null at any measured baseline. The departures from a uniform disc model are much greater than at 1290 nm, and the small visibilities (~3 per cent) near the baseline corresponding to the secondary maximum of the uniform disc model suggest either a strongly limb-darkened radial intensity profile, or a model including a compact component at just the right location to give small visibility amplitudes on these particular baselines.

More importantly, the closure phases show the unambiguous signature of asymmetry, with most measurements significantly different from the zero or 180° values expected for a symmetric source. On baselines shorter than the location of the visibility minimum near 5.5 m the closure phases have values of ~20°, but beyond this minimum most of the values are close to 130°. Two features of the data provide further information on the type of structure present: the small visibilities on long baselines constrain

Table 2. Best-fitting one-spot models for Betelgeuse as observed on 1997 November 21 at 905 nm. The models consist of a limb-darkened disc with one (bright or dark) unresolved feature superimposed. The coordinates (r, θ) give the position of the unresolved feature (modelled as a finite-sized circular Gaussian) with respect to the centre of the underlying disc. θ is measured north through east. The notation FDD refers to the Hestroffer fully-darkened disc component. For Gaussian components, 'diameter' refers to the FWHM and a negative flux indicates a dark feature. Parameters for which no uncertainty is quoted were fixed during the fitting process.

χ^2	Component	Flux	r (mas)	θ (°)	Diameter (mas)
4.3	FDD ($\alpha = 4$)	0.95	–	–	71.0 ± 0.7
	Gaussian	0.027 ± 0.003	5.9 ± 1.0	119 ± 5	10
3.9	FDD ($\alpha = 4$)	0.95	–	–	68.0 ± 0.8
	Gaussian	-0.029 ± 0.004	8.6 ± 1.1	-31 ± 7	10

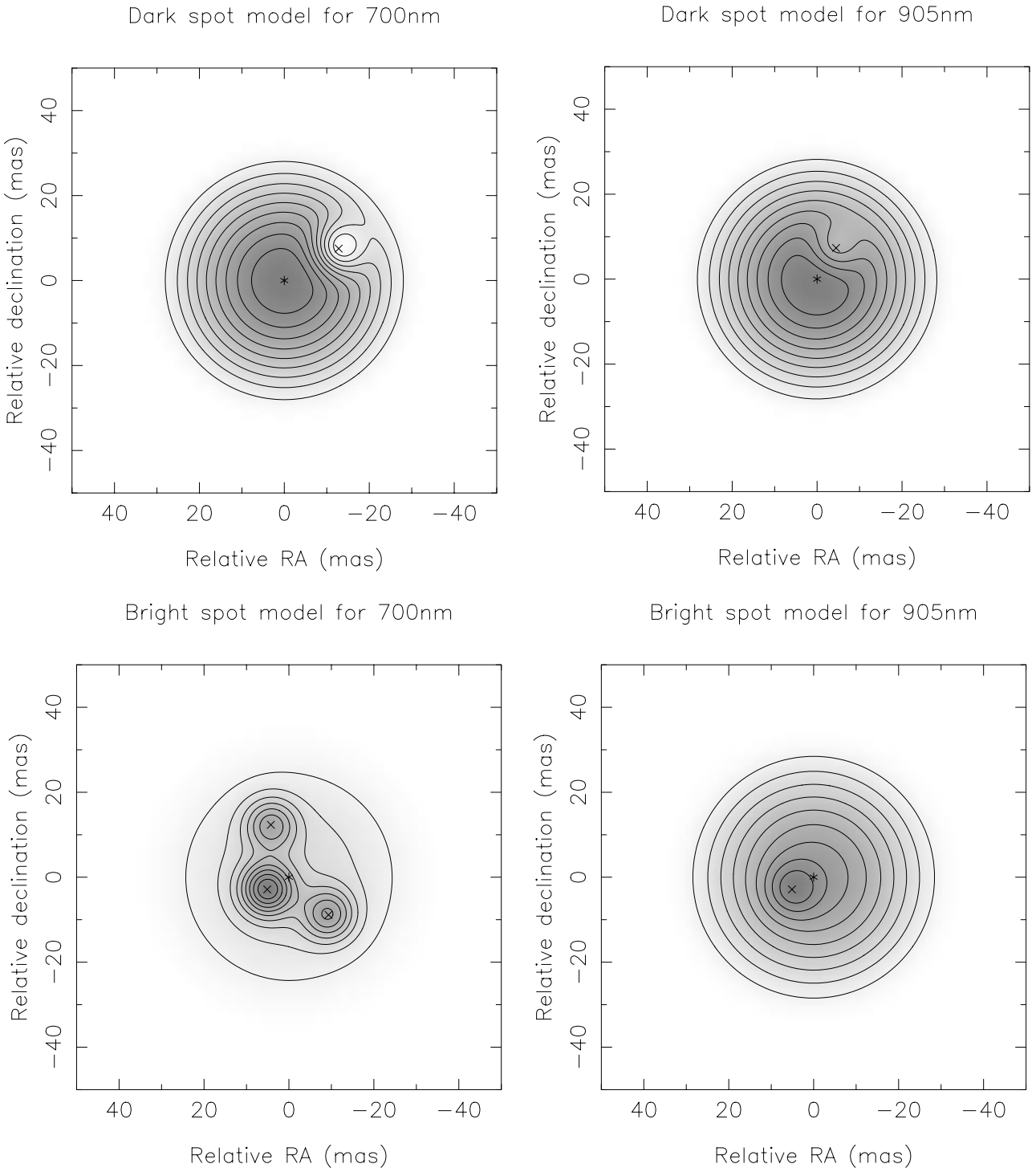

Figure 3. Brightness distributions for the best-fitting models with dark features (top) and bright features (bottom). The models for the 700-nm data are on the left and those for 905 nm are on the right. Note the greater asymmetry at the shorter of the two wavelengths. The brightest areas are shaded darkest. The sizes of the features are unconstrained by the data. To generate these plots, the features were assumed to be Gaussian with FWHM = 10 mas. North is up and east is to the left. The contours are at 10, 20, 30, …, 90 per cent of the peak brightness. Parameter values for the models are listed in Tables 2 and 3.

the amount of unresolved flux that can be present, and the fact that on long baselines the closure phases vary by less than 20°, while the position angle on the sky of the longest baseline changes by 30°, implies that any compact features must be located close to the centre of the star.

Table 2 presents the results of our model fitting at 905 nm. Simple symmetric limb-darkened disc models were unable to describe the closure phase measurements adequately, but the addition of a single unresolved bright or dark spot to a strongly limb-darkened disc (α in the range 3–4) allowed reasonable fits to both the visibility amplitude and closure phase data. The best-fitting parameters for models incorporating a limb-darkened disc with $\alpha = 4$ are given in Table 2, which shows results for both a bright and dark (negative flux) 'spot'. In both cases it was

necessary to fix the disc flux (rather than treat it as a free parameter) to constrain the visibility to be consistent with the WHT observations at the same wavelength. In practice, the brightness distributions implied by the two different models were very similar (see Fig. 3): the dark spot is located at a position angle 150° lower than that of the bright spot, but is at a similar radius, and contributes a similar fraction of the total flux (3 per cent).

As can be seen from Table 2 a number of the parameters describing the models were fixed during the model fitting, notably the sizes of the compact components (10 mas) and the limb-darkening parameter, α. The volume of COAST data available at 905 nm did not allow these to be determined independently, and so where possible other workers' results were used to estimate appropriate values for these parameters. Although our data rule out the extremes of either uniform or Gaussian intensity profiles for the disc component, a range of values for α between 2 and 5 were consistent with the measurements. The particular choice for α adopted has been based on the measurements of Burns et al. (1997) whose 830/40-nm brightness profile of Betelgeuse, measured in 1995 October, is reasonably well fit with α equal to 3.7 ± 0.1. The similarity of their bandpass to the 905/50-nm bandpass used here, both in terms of central wavelength and expected line blanketing, implies that the results of Table 2 are unlikely to have been biased significantly by setting α equal to four. Other models consistent with our data, although with slightly weaker limb darkening, typically gave larger flux contributions from the compact features, but in no case did this exceed 5 per cent of the total. Increasing the sizes of the compact features had a similar effect – full-width half-maxima as large as 20 mas could not be excluded on the basis of the value of χ^2 alone – but at most led to 8 per cent of the total flux originating from any compact structure.

One final point that deserves mention is a potential ambiguity that can arise from correlations between the locations and relative fluxes of the compact features seen on Betelgeuse. Previous authors using relatively short ($\leqslant$4 m) interferometer baselines (Wilson et al. 1992; Tuthill et al. 1997; Wilson et al. 1997) have often found that identical closure phase signatures can be produced by bright centrally located features and by fainter features at greater radial distances. This ambiguity does not arise here, since the visibilities measured on long ($\geqslant$5 m) baselines, where the contribution from the limb-darkened disc is low, imply that the flux from any single feature must be small.

3.2.3 *Asymmetries at 700 nm*

Signatures of the asymmetric component to Betelgeuse's brightness distribution in 1997 November were most evident at 700 nm. Here, although the interferometer baselines were unable to fully resolve the star (see Fig. 4), the large number of very accurately measured closure phases bear the distinctive hallmarks of compact features located within the stellar disc. Furthermore, the visibility data alone show marked deviations from a uniform disc model.

The lack of visibility amplitude measurements on baselines longer than 4 m meant that no information could be gleaned about the limb darkening of Betelgeuse at 700 nm, and so for consistency with our 905-nm results, most of the modelling was performed using a value of α of four. Fortunately, the derived characteristics of the compact model components were found to depend insignificantly on the precise value of α, and so the results presented here will be reasonably unbiased. Given the complexity of the closure phase variations, it was not possible to fit the 700-nm measurements with any model consisting of either one or two bright compact components superimposed on a limb-darkened disc. Models incorporating three bright spots were, however, successful and although several minima with comparable χ^2 values were found in the 11-dimensional solution space, all were qualitatively similar with hotspot fluxes ranging between 7 and 16 per cent of the total flux. A fit with only a marginally higher value of χ^2 could also be achieved by constraining one of the bright features to be located at the preferred position of the bright feature inferred from the 905-nm data (see Table 2). The parameters of this 700-nm model are given in Table 3. Most importantly, it was not possible to fit the data with any model in which the hotspot fluxes were just a few per cent of the total.

Table 3 also lists the details of an alternative parametrization of the brightness distribution involving a dark spot. In the past, this type of model has not been favoured since larger numbers of free parameters have been required to fit the observations than models using bright spots (see, e.g. Wilson et al. 1997; Tuthill, Haniff & Baldwin 1999). This does not happen here but, as for the 905-nm model fitting, the hotspot and dark-spot models both predicted very similar overall brightness distributions. For both types of models, the sizes of the unresolved components were not well constrained by the 700-nm data, which imply an upper limit of ~15-mas FWHM.

As a check on the reliability of the model fitting, the data at

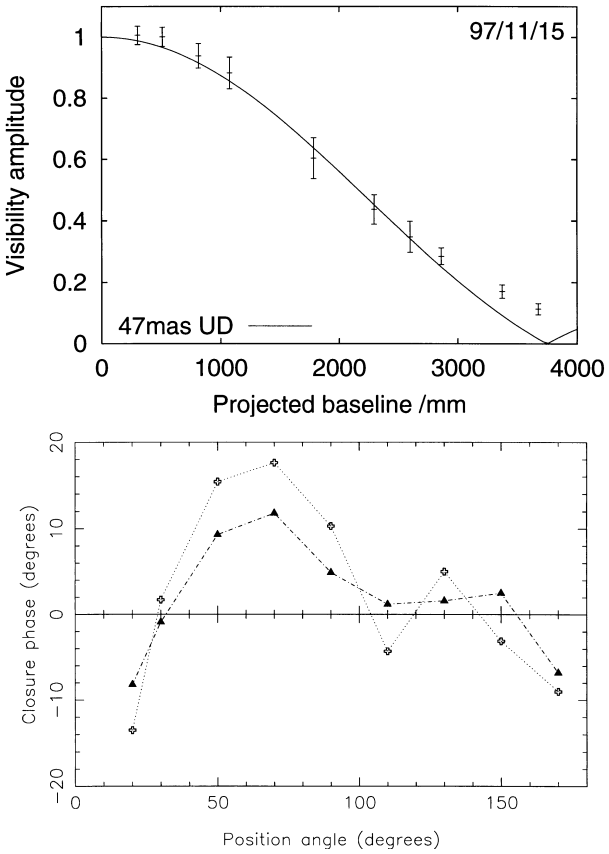

Figure 4. Azimuthally averaged visibility amplitudes, and closure phases measured for Betelgeuse on 1997 November 15 at 700 nm with the WHT. Each visibility datum is the average of nine measurements made at different position angles on the sky. The solid curve in the top panel is the visibility function predicted for a uniform disc of diameter 47 mas. The closure phases on two of the 10 measured triangles of baselines have been plotted as a function of the position angle of the aperture mask on the sky in the lower panel. The errors on the closure phases are ~2°.

Table 3. Best-fitting models for Betelgeuse on 1997 November 15 at 700 nm. As for the model fitting at 905 nm, the source is described as a limb-darkened disc with one or more superimposed (bright or dark) unresolved features. The entries in the table are as described in Table 2.

χ^2	Component	Flux	r (mas)	θ (°)	Diameter (mas)
3.0	FDD ($\alpha = 4$)	0.68 ± 0.07	–	–	76 ± 5
	Gaussian	0.08 ± 0.02	13.0 ± 1.1	19 ± 4	10
	Gaussian	0.13 ± 0.02	5.9	119	10
	Gaussian	0.09 ± 0.02	12.9 ± 1.1	226 ± 4	10
3.1	FDD ($\alpha = 4$)	1.05 ± 0.05	–	–	67.8 ± 0.5
	Gaussian	-0.06 ± 0.01	14.8 ± 0.4	-59.6 ± 1.0	10

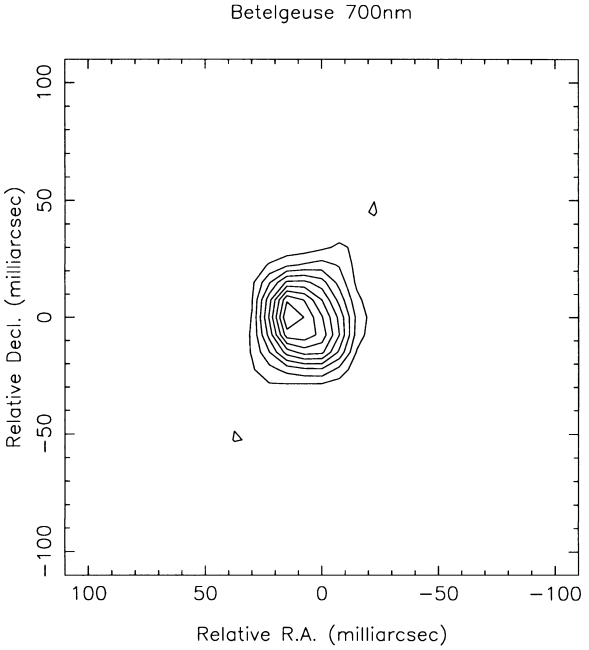

Figure 5. Reconstructed image of Betelgeuse, from WHT data taken on 1997 November 15 at a wavelength of 700 nm. North is up and east is to the left. The contours are at 10, 20, 30, …, 90 per cent of the peak flux. This image is highly asymmetric, in good agreement with independent model fitting to the dataset.

700 nm were inverted using a radio-astronomical self-calibration code incorporating maximum entropy deconvolution (Sivia 1987). The resulting image is shown in Fig. 5. Although the dynamic range in the image is low (∼20 : 1), owing to poor calibration of the visibility amplitudes, the map confirms that the star appeared highly asymmetric at this wavelength and epoch, with the eastern half of the disc appearing brightest, and the north-west region appearing least bright. This distribution of flux agrees well with that inferred from the model fitting, and attests to the crucial role played by measurements of closure phases in elucidating the source structure reliably.

3.2.4 Wavelength dependence

The results of the previous sections demonstrate that the asymmetric structure seen in Betelgeuse showed considerable wavelength dependence in 1997 November. To test whether or not the combined datasets at 1290, 905 and 700 nm were compatible with a single brightness distribution, models with both bright and dark spots, fixed at locations derived from the 700-nm measurements, were fit to the 1997 November 21 905-nm data and to the 1997 November 11 1290-nm data. At 905 nm, none of the three-spot models which gave good fits at 700 nm was satisfactory, unless the contributions of two of the three spots were reduced to insignificant levels ($\lesssim$1 per cent of the total flux). Similarly, the single dark-spot model provided a very poor representation of the source at 905 nm, unless the spot was moved inwards by ∼5 mas. At 1290 nm, a similar mismatch was evident, there being no evidence for the presence of any of the bright or dark features at a level of >2 per cent of the disc flux.

Our measurements are thus compatible with a star whose appearance was very different at the three wavelengths at which it was observed, with a large asymmetry apparent at 700 nm, a small one at 905 nm and no detectable asymmetry seen at 1290 nm. Our models for the star are summarized in Fig. 3 which shows the brightness distributions inferred for the models with either dark features (top) or bright features (bottom) that were found to best fit the 700 (left) and 905-nm (right) data. As expected, the brightness distributions for the two 700-nm models have a similar appearance, as do those for the two 905-nm models.

3.3 Limb-darkening

The model fitting described above was also used to investigate the limb-darkening function of Betelgeuse. Not surprisingly, the strongest constraints come from the measurements at 1290 and 905 nm, which extend beyond the first null in the visibility function. Using Hestroffer's (1997) parametrization, the visibility amplitudes at 1290 nm (where the effects of asymmetric structure were insignificant) were very well fit by an α value of 1.3 ± 0.1 and a zero-intensity disc diameter of 51.4 ± 0.8 mas. This model and data are presented in Fig. 6, which also shows the topology of the χ^2 surface in the region of its minimum value. This indicates that these new measurements do indeed constrain both α and the disc diameter reasonably well, despite the correlation between the two parameters. For comparison, the near-infrared measurements could also be fit (equally well) using a standard linear limb-darkening law:

$$I(r) = 1 - \alpha_1(1 - \mu), \tag{1}$$

with $\alpha_1 = 1.25 \pm 0.12$ and a diameter of 52.6 ± 1.6 mas. Here $\mu = \cos\theta$, with θ the angle between the line of sight and the radial vector from the centre of the star. The difference between this representation and that of a Hestroffer model with a limb-darkening parameter of one is small, but is most pronounced near the stellar limb where the intensity goes negative, highlighting the inadequacy of linear models for strongly limb-darkened discs (see, e.g. Burns et al. 1997).

The radial intensity profile inferred at 905 nm was far less flat-topped than at 1290 nm, and was best fit with a Hestroffer model

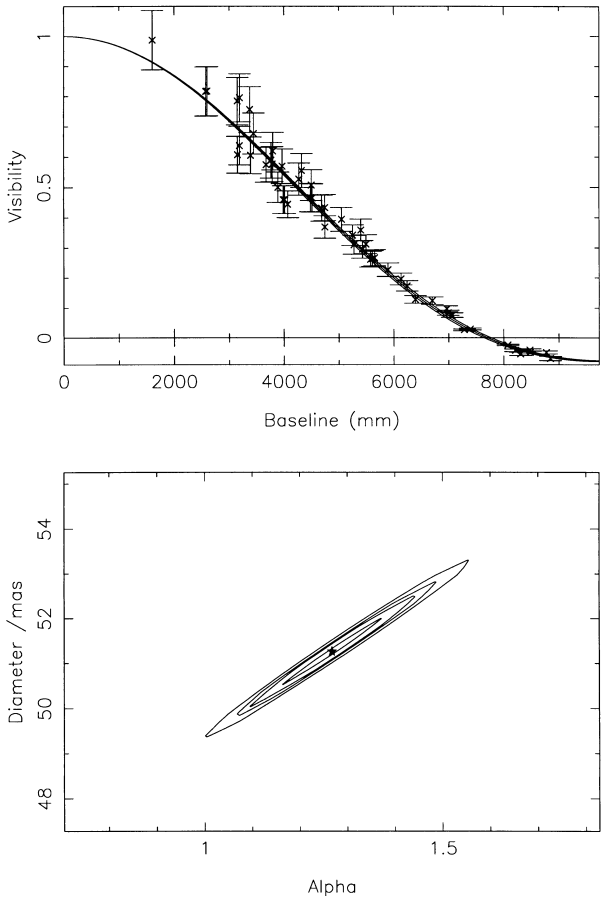

Figure 6. Best-fitting two-parameter Hestroffer limb-darkened disc model for Betelgeuse at a wavelength of 1290 nm. The upper plot shows the visibility data (note that the signs of the visibility points have been inferred from the closure phase data), the best-fitting model and the $\pm 3\sigma$ fits. The bottom plot shows the negative logarithm of the posterior probability of the model (equal to $\chi^2/2 +$ constant). Contours are plotted at 68.3, 90, 95.4 and 99 per cent confidence intervals.

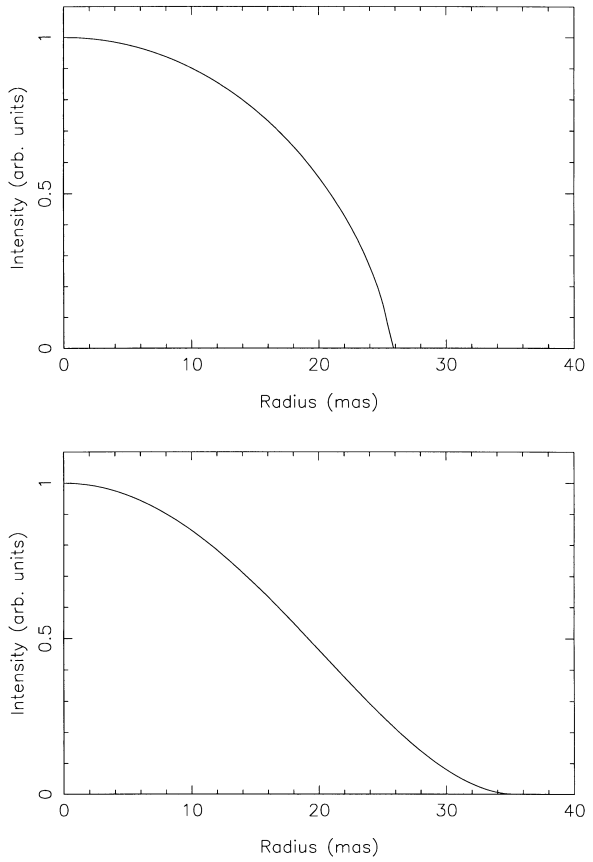

Figure 7. Best-fitting radial intensity profiles for Betelgeuse at 1290 (top) and 905 nm (bottom). Note the much larger extent and greater limb-darkening present at the shorter wavelength.

with a value for α of between 3 and 4 (see Section 3.2.2). The differences in the appearance of Betelgeuse at these two wavelengths are most clearly seen in the deduced radial intensity profiles, shown in Fig. 7. The larger size and softer decline to zero intensity at 905 nm are very clear in this representation, and suggest that even at 905 nm interferometric measurements are unlikely to be probing the deeper photospheric layers in the star.

4 DISCUSSION

4.1 A simple convective hotspot model

In the past, the bright features seen on the disc of Betelgeuse have been accounted for in terms of a simple model where a small number of large convective granules are present on the stellar surface. These are assumed to give rise to regions of enhanced temperature that change on time-scales of months (see, e.g. Buscher et al. 1990; Wilson et al. 1992; Tuthill et al. 1997). However, the limited angular resolution and narrow range of wavelengths used in the past (633, 700 and 710 nm) have meant that it has been difficult to constrain both the angular size and temperature of these hotter regions. The best measurements to date have implied sizes of <20 per cent of the disc area and corresponding temperature excesses of >400 K. The simultaneous multi-wavelength observations presented here allow a new and more direct test of this model.

The model fitting outlined in Section 3.1 yields a description of the brightness distribution in which a disc and a number of spots are superposed. In this case the spot emission is simply the excess emission from the warm region above that of the surrounding disc. We can thus define an observable spot contrast, r_λ, which is equal to the ratio of the flux of a spot component to that of the disc in any given model. If we assume that both the stellar surface and the hotter zones radiate as blackbodies, then r_λ can be written as:

$$r_\lambda = \frac{A_\mathrm{h}[P(\lambda, T_\mathrm{h}) - P(\lambda, T_*)]}{A_* P(\lambda, T_*)}, \qquad (2)$$

where A_h and A_* are the hotspot and disc areas respectively, $P(\lambda,T)$ is the Planck function, and T_h and T_* refer to the hotspot and disc temperatures. The distinction between the flux from a superimposed 'hotspot' model component and the flux from the corresponding hot region of the stellar surface is illustrated graphically in Fig. 8.

Following previous workers and adopting a disc temperature for Betelgeuse of 3500 K, we have computed the values expected for the spot contrast r_λ, for a range of excess spot temperatures and values of A_h/A_*. These are summarized in Table 4 and compared with the spot contrast observed for the most prominent feature seen on Betelgeuse, i.e. the brightest feature shown in Fig. 3. Although the table presents results for only a limited region of parameter space, the general behaviour of this model is clear.

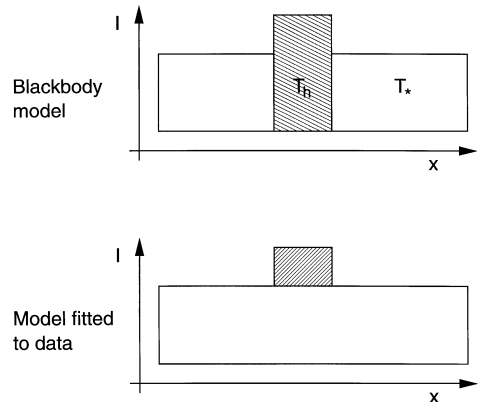

Figure 8. Illustration of the distinction between the hotspot in the model obtained from a fit to the Fourier data, and that in the physical blackbody model intended to represent the underlying origin of the stellar emission. See text for explanation.

First, for hotspots with small temperature excesses, unreasonably large surface areas (>25 per cent) are required to match the observed spot contrast at 700 nm. Secondly, although smaller and hotter regions on the stellar surface can fit the observations at 700 nm, in all cases significantly larger contrast ratios are predicted than observed at 905 and 1290 nm. In short, no combination of reasonable disc and hotspot temperatures and hotspot areas can reconcile this simple model with the observations: the featureless appearance of Betelgeuse seen in the near-infrared is inconsistent with the strong asymmetries seen at 700 nm.

Table 4. Predicted spot-contrasts r_λ for spots with differing fractional areas A_h/A_* and temperatures T_h, computed for a disc temperature of 3500 K. In this simple model, both the spot and disc are assumed to radiate as blackbodies and the ratio A_h/A_* is independent of wavelength. Note that in all cases the relative spot contrast between the shortest and longest wavelength is roughly a factor of two.

A_h/A_*	T_h	r_λ 700 nm	905 nm	1290 nm
0.25	3700	0.09	0.07	0.05
0.25	3800	0.15	0.11	0.08
0.23	3900	0.19	0.14	0.09
0.17	4000	0.19	0.13	0.09
0.14	4100	0.19	0.14	0.09
0.12	4200	0.20	0.14	0.09
0.10	4300	0.20	0.14	0.09
0.08	4400	0.19	0.13	0.08
Observed		0.19 ± 0.03	0.028 ± 0.003	<0.02

Table 5. Predicted spot-contrasts r_λ for spots with differing fractional areas A_h/A_* as measured at 700 nm and temperatures T_h, computed for a disc temperature of 3500 K at 1290 nm. In this revised model the effective disc temperature is 3230 K at 905 nm and 2960 K at 700 nm, and the disc diameters are in the ratio 1.00 : 0.81 : 0.72 at 700, 905 and 1290 nm respectively.

A_h/A_* at 700 nm	T_h	r_λ 700 nm	905 nm	1290 nm
0.10	3500	0.19	0.031	0.000
0.09	3540	0.19	0.032	0.001
0.08	3600	0.19	0.035	0.004
0.05	3820	0.19	0.038	0.008
0.02	4460	0.19	0.039	0.011
Observed		0.19 ± 0.03	0.028 ± 0.003	<0.02

4.2 A modified hotspot model

While our new data rule out the simplest of models described above, there are two important effects that any more realistic model must clearly take account of. First, that the apparent diameter of Betelgeuse is different at different wavelengths (see, e.g. Balega et al. 1982 for measurements of Betelgeuse, and Quirrenbach et al. 1993 for measurements of other cool giants) and, secondly, that, owing to significant line blanketing, its spectrum cannot be well fit by a single blackbody. To accommodate the first of these, we have fit uniform disc models to the short-baseline (i.e. within the first null) visibility functions of Betelgeuse to obtain preliminary estimates of the stellar 'diameter'. Any estimate of the apparent diameter at 700 nm must take into account the presence of hotspots contributing ~30 per cent of the total flux. Hence a model consisting of a uniform disc plus three hotspots was employed at this wavelength, to yield a disc diameter of 59 ± 3 mas. Diameters of 47.8 ± 0.3 and 42.6 ± 0.1 mas were obtained for the 905 and 1290-nm wavebands respectively. These estimates were not corrected for the insignificant effects of any low-level unresolved structure. The smaller apparent diameters reflect the reduced effects of blanketing in the near-infrared.

To evaluate the effective blackbody flux from the stellar disc at each wavelength, we have used a 'typical' M3III spectrum from the catalogue of Pickles (1998) to calibrate the relative fluxes expected from Betelgeuse in the three measured bandpasses. Pickles' catalogue contains no M2Iab supergiant spectrum as would be required to match Betelgeuse's spectral characteristics precisely, but for this first-order correction, a giant spectrum will suffice. The relative fluxes were then combined with the measured diameter estimates to yield effective blackbody temperatures, T_λ, at each wavelength on the assumption that at 1290 nm the emission from Betelgeuse arises from an unobscured blackbody at 3500 K. The resulting blackbody temperatures were 3230 ± 10 K at 905 nm and 2960 ± 40 K at 700 nm, the cooler temperatures reflecting once again the increased opacity at shorter wavelengths resulting from molecular and atomic species.

Table 5 shows the predictions of this revised model for the region of parameter space whose predictions are closest to our observations. Physically, this new model includes the effects of wavelength-dependent opacity on the disc contribution to the brightness distribution, but assumes, as before, that emission from the hotspot reaches the observer essentially unobscured. In this case the fit between data and model is much better than before, although the data do not allow the size and temperature of the hotspots to be determined independently. If the size of the hotspot is 10 per cent of the disc area at 700 nm, this implies a hotspot temperature equal to the 1290-nm disc temperature. Smaller hotspot areas imply higher hotspot temperatures. In the context of this model, then, the principal cause for the large changes in apparent spot contrast with wavelength is not the wavelength dependence of the blackbody function, but rather the effective reduction in the disc brightness owing to opacity effects. These are relatively small in the near-infrared but much stronger in bandpasses that are contaminated by TiO and other molecular and atomic species, such as the 700 and 905-nm bandpasses used here.

One requirement of this model that deserves emphasis is the

need for the hotspot emission to escape from the star without being subject to the same blanketing as radiation from the deeper photosphere. In principle, this could imply that the hotspot emission arises from a zone in the outer stellar atmosphere, but the data presented here do not allow any resolution of this question. Perhaps a more plausible scenario is one in which processes at the stellar surface perturb the overlying atmosphere and alter its opacity along the line of sight to the observer. There is some indirect evidence that large convective plumes can extend into the outer atmosphere of Betelgeuse, e.g. Lim et al. (1998) suggest that convection is the mechanism by which the asymmetrically-distributed circumstellar gas they detect is transported from the photosphere of the star, and so one possibility would be that these, together with localized heating, lead to less opaque channels through which the emission from the photosphere can escape.

Although detailed modelling of the response of a cool supergiant atmosphere to thermal and dynamical perturbations is probably required to investigate this type of model quantitatively, at least two relatively straightforward observational tests can be envisaged. First, at any given epoch, large variations in spot contrast should be visible crossing deep spectral features. Previous experiments (Buscher et al. 1990; Wilson et al. 1992; Tuthill et al. 1997) have revealed only small differences in hotspot contrast between 700 (near-continuum) and 710-nm (strong TiO absorption) bandpasses. However, for these experiments relatively broad (10-nm FWHM) filters were used and it is possible that significant leakage of continuum flux may have affected the 710-nm measurements. The fact that the disc diameters measured at 700 and 710 nm did not differ substantially supports this suggestion, and highlights the need for further measurements in narrower bandpasses.

A second test will be to search for correlations between variations in the hotspot fluxes and TiO strength. The strength of the TiO absorption bands in Betelgeuse is known to vary irregularly (see, e.g. Morgan, Wasatonic & Guinan 1997), and so periods during which asymmetries were not present on Betelgeuse might be expected to occur during phases of unusually low TiO strength.

4.3 Limb darkening

Given the relative paucity of direct limb-darkening measurements (Hanbury Brown et al. 1974; Quirrenbach et al. 1996; Burns et al. 1997) it is interesting to compare the linear limb-darkening coefficient determined from our 1290-nm COAST measurements with theoretical predictions in the literature, with the caveat that most model atmospheres are more appropriate to giant stars than supergiants. In an early paper Manduca (1979) obtained $\alpha_1 = 0.52$ from a least-squares fit to the intensity profile (in a narrow passband centred on 1.2 μm) of a model star with $T_{\rm eff} = 3750$ K, $\log g = 1.5$ and solar composition. More recently Van Hamme (1993) has predicted $\alpha_1 = 0.49$ for the J band limb-darkening coefficient of a model with $T_{\rm eff} = 3500$ K, $\log g = 0.5$ and solar composition. Our measured value for Betelgeuse (which has $\log g \sim 0$ and $T_{\rm eff} \sim 3500$ K) has $\alpha_1 = 1.25 \pm 0.12$ and so it is clear that Betelgeuse appears more strongly limb-darkened at 1.3 μm than both these models predict.

A further anomaly arises when we compare the zero-intensity diameter of Betelgeuse at 1.3 μm with the 11-μm uniform disc measurement of Bester et al. (1996). At this wavelength any limb-darkening corrections should be negligibly small (~1 per cent) and so a uniform brightness distribution should be an appropriate model to fit. Their measurement of 56 ± 1 mas is 9 per cent larger than the corresponding diameter measured at COAST at 1.3 μm. Thus, either these two bandpasses sample quite different layers in the stellar atmosphere, or the discrepancy points to a real change in the stellar diameter between the two measurement epochs. The lack of asymmetry seen at 1.3 μm suggests that future interferometric monitoring at infrared wavelengths could be used to quantify any size changes of this order perhaps associated with radial pulsation.

5 SUMMARY

Contemporaneous interferometric imaging observations of Betelgeuse obtained in 1997 October–November have revealed very different apparent morphologies in three widely-separated wavebands at 700, 905 and 1290 nm. At 700 nm the visibility and closure phase data can be interpreted in terms of a disc with either three bright features or one dark feature superimposed, although the dark spot interpretation appears less likely given previous observations. At 905 nm a smaller asymmetry was detected, whereas at 1290 nm the apparent brightness distribution was highly symmetric.

If the asymmetries are modelled as bright features superimposed on a circular disc, the changes in contrast with wavelength are inconsistent with the bright features simply being areas of elevated temperature on the surface of the star. We suggest a revised model which accommodates the geometrically-extended and line-blanketed atmosphere of Betelgeuse, in which the features are seen along lines of sight for which the atmospheric opacity has been reduced as the result of activity (e.g. convection) at the stellar surface. In this picture the contrast of the features is enhanced at wavelengths where significant sources of opacity, e.g. TiO, are present. The resulting bright features then evolve in the same way as the underlying activity, providing a simpler explanation for changing hotspot locations than models requiring interactions between shock waves, or non-radial pulsation. Imaging in other, narrower bands, both at wavelengths of strong TiO absorption and in the continuum, should provide useful tests of this revised hotspot model.

We have empirically identified the 1.3-μm waveband as being uncontaminated by asymmetries in the stellar brightness distribution, and therefore useful for future measurements of any diameter changes caused by stellar pulsation.

ACKNOWLEDGMENTS

The authors would like to thank Dr J. Lehar for modifying his versions of two of the Caltech VLBI software programs. We are grateful to the Royal Society (CAH), to NSERC Canada and the CSA (DSJ) for financial support, and to G. Charbaut for valuable contributions. The William Herschel Telescope is operated on the island of La Palma by the Royal Greenwich Observatory in the Spanish Observatorio del Roque de los Muchachos of the Instituto de Astrofísica de Canarias.

REFERENCES

Baldwin J. E., Haniff C. A., Mackay C. D., Warner P. J., 1986, Nat, 320, 595

Baldwin J. E. et al., 1994, Proc. SPIE, 2200, 118

Balega Y., Blazit A., Bonneau D., Koechlin L., Foy R., Labeyrie A., 1982, A&A, 115, 253
Bester M., Danchi W. C., Hale D., Townes C. H., Degiacomi C. G., Mékarnia D., Geballe T. R., 1996, ApJ, 463, 336
Burns D., 1997, PhD thesis, Univ. Cambridge
Burns D. et al., 1997, MNRAS, 290, L11
Buscher D. F., Haniff C. A., Baldwin J. E., Warner P. J., 1990, MNRAS, 245, 7P
Gilliland R. L., Dupree A. K., 1996, ApJ, 463, L29
Hanbury Brown R., Davis J., Lake R. J. W., Thompson R. J., 1974, MNRAS, 167, 475
Haniff C. A., Mackay C. D., Titterington D. J., Sivia D., Baldwin J. E., Warner P. J., 1987, Nat, 328, 694
Hestroffer D., 1997, A&A, 327, 199
Hofmann K.-H., Scholz M., 1998, A&A, 335, 637
Klückers V. A., Edmunds M. G., Morris R. H., Wooder N., 1997, MNRAS, 284, 711
Lim J., Carilli C. L., White S. M., Beasley A. J., Marson R. G., 1998, Nat, 392, 575
Manduca A., 1979, A&AS, 36, 411
Morgan N. D., Wasatonic R., Guinan E. F., 1997, Inf. Bull. Var. Stars, 4499
Pickles A. J., 1998, PASP, 110, 863
Quirrenbach A., Mozurkewich D., Armstrong J. T., Buscher D. F., Hummel C. A., 1993, ApJ, 406, 215
Quirrenbach A., Mozurkewich D., Buscher D. F., Hummel C. A., Armstrong J. T., 1996, A&A, 312, 160
Schwarzschild M., 1975, ApJ, 195, 137
Sivia D. S., 1987, PhD thesis, Univ. Cambridge
Tuthill P. G., Haniff C. A., Baldwin J. E., 1997, MNRAS, 285, 529
Tuthill P. G., Haniff C. A., Baldwin J. E., 1999, MNRAS, 306, 353
Uitenbroek H., Dupree A. K., Gilliland R. L., 1998, AJ, 116, 2501
Van Hamme W., 1993, AJ, 106, 2096
Wilson R. W., Baldwin J. E., Buscher D. F., Warner P. J., 1992, MNRAS, 257, 369
Wilson R. W., Dhillon V. S., Haniff C. A., 1997, MNRAS, 291, 819
Young J. S., 1999, PhD thesis, Univ. Cambridge
Young J. S. et al., 1998, Proc. SPIE, 3350, 746

This paper has been typeset from a TEX/LATEX file prepared by the author.